Journal of Power Sources 231 (2013) 203–212

Contents lists available at SciVerse ScienceDirect

Journal of Power Sources

journal homepage: www.elsevier.com/locate/jpowsour

Study of calcium–magnesium–aluminum–silicate (CMAS) glass and glass-ceramic sealant for solid oxide fuel cells

Allu Amarnath Reddy [a], Ashutosh Goel [a,b], Dilshat U. Tulyaganov [a,c], Saurabh Kapoor [a], K. Pradeesh [d], Maria J. Pascual [e], José M.F. Ferreira [a,*]

[a] Department of Materials and Ceramics Engineering, University of Aveiro, CICECO, Campus Santiago, 3810-193 Aveiro, Portugal
[b] Sterlite Technologies Ltd., E1, E2, E3, MIDC Waluj, Aurangabad 431136, India
[c] Turin Polytechnic University in Tashkent, 17, Niyazova Str., 100095 Tashkent, Uzbekistan
[d] Optoelectronics Research Centre, University of Southampton, SO17BJ, UK
[e] Instituto de Cerámica y Vidrio (CSIC), C/Kelsen 5, Campus de Cantoblanco, 28049 Madrid, Spain

HIGHLIGHTS

- ► Calcium–magnesium–aluminum–silicate based GCs were evaluated for sealant materials.
- ► Investigated glass-ceramics are showing stable CTE values.
- ► Obtained Weibull modulus points out to good reliability of the sealing process.
- ► The glasses were found to be chemically compatible with SOFCs components.

ARTICLE INFO

Article history:
Received 12 October 2012
Received in revised form
12 December 2012
Accepted 14 December 2012
Available online 8 January 2013

Keywords:
Coefficient of thermal expansion
Thermal stability
Interaction
Interconnect

ABSTRACT

A parent glass within the CaO–MgO–Al_2O_3–SiO_2 system and resulting glass–ceramics (GCs) have been appraised for solid oxide fuel cells (SOFCs) sealing applications. The sintering behavior was investigated by differential thermal analysis and hot stage microscopy. The glass composition exhibited single-stage shrinkage behavior with high sintering ability, and a suitable viscosity of $10^{7.1}$ dPa s at the SOFCs operating temperature 900 °C. X–ray diffraction in conjunction with the Rietveld–RIR technique were employed to quantify the crystalline and amorphous phases in the GCs sintered at 900 °C for 1 h and 850 °C for 300 h. The coefficients of thermal expansion (CTE) measured were 9.7×10^{-6} K^{-1} (200–500 °C) and $\sim 10.1 \times 10^{-6}$ K^{-1} (200–700 °C) for glass and GCs, respectively, in good agreement with those typical for SOFC components. Weibull analysis was applied on the three-point bend data of GCs in order to obtain the mechanical strength distribution, characteristic strength and Weibull modulus. Well matching CTE, flexural strength values, good sintering behavior and adhesion to the other components in air atmosphere allow proposing this glass composition as promising candidate for further experimentation as sealant for SOFCs.

1. Introduction

The vital requirement for the modern world is the efficient production of electricity. On the other hand, the depletion of fossil fuel reserves and the emission of greenhouse gases constitute a menace to the present and the future generations in terms of energy availability, environmental pollution, global warming and health hazards. Hydrogen has been identified as a potential alternative fuel as well as an energy carrier for the current and future energy supply. Due to the ability of solid oxide fuel cells (SOFCs) to operate by using conventional hydrocarbon fuel (biomass, hydrogen), SOFCs can play a critical role in both current and future energy solutions. In addition to fuel flexibility, SOFCs are 45–65% efficient (total system efficiency ~85%) in the conversion of fuel to electricity unheard of by any other technology. Among different SOFC designs, the planar type, which is cost effective and mechanically robust, offers an attractive potential for increase the power density compared to other fuel cells. However, many technical hurdles need to be overcome before commercializing this technology. One of the most arduous tasks in commercializing SOFC

* Corresponding author. Tel.: +351 234 370242; fax: +351 234 370204.
E-mail address: jmf@ua.pt (J.M.F. Ferreira).

0378-7753/$ – see front matter © 2012 Elsevier B.V. All rights reserved.
http://dx.doi.org/10.1016/j.jpowsour.2012.12.055

is the development of a hermetic seal in which can prevent gases from mixing in the anode and the cathode, and has the ability to provide electrical insulation in order to avoid shunting [1–4].

Since a p-SOFC works at a high temperatures (800–1000 °C) and its components are exposed to both oxidizing and reducing gas atmospheres, the sealant for the SOFC needs to exhibit several special characteristics; for instance, the seals must have a CTE similar to those of other cell components (9–12) $\times 10^{-6}$ K^{-1}; be stable in a wide range of oxygen partial pressure (air and fuel) and be chemically compatible with other fuel cell components, while minimizing thermal stresses during high-temperature operation. These demands constitute a major challenge in the development of p-SOFCs. Most recently, there has been a dramatic revival of interest in both glass-and glass-ceramic (GC)-to-metal seals, particularly for new applications including sealants in SOFC and other high temperature electrochemical applications. The main motivations behind are meeting most of the SOFCs seal requirements with carefully tailored chemical composition [5–7]. Substantial work is under progress in this area, aiming at improving the performance of these sealants under extreme operating conditions of current fuel cell designs, which involve both high temperatures and highly corrosive environments.

Pacific Northwest National Laboratory (PNNL) patented a glass-based sealant named as G18 (15CaO–35BaO–5Al_2O_3–10B_2O_3–35SiO_2 (mol.%)) that has been widely used [8]. Mahapatra and Lu [9] claimed for a glass composition in the system SrO–La_2O_3–Al_2O_3–SiO_2 comprising (mol.%) (40(SrO:La_2O_3:Al_2O_3)–60SiO_2) exhibiting desired thermo physical properties. However, the proneness of G18 glass for crystallizing the low thermal expansion monoclinic celsian ($BaAl_2Si_2O_8$) phase during long term SOFC operation, its high BaO content that might also react with Cr-vapors (CrO_3 or $CrO_2(OH)_2$) diffused to the glass surfaces to form $BaCrO_4$, constitute the most serious drawbacks as SOFC sealant. The large CTE differences between this chromate ($\sim$18–20 $\times$ 10^{-6} K^{-1}), the sealing glass (CTE 10–13 $\times$ 10^{-6} K^{-1}) and the interconnect ($\sim$11–13 $\times$ 10^{-6} K^{-1}) lead to significant losses in bonding strength between SOFC glasses and interconnect materials or to their physical separation. On the other hand, the glass sealant proposed by Mahapatra and Lu [9] still needs to be tested in actual SOFC cells for long term under realistic dual atmosphere conditions. The difficulties in meeting all the requirements in a given material stimulated Union Research Center of Fuel Cell in China University of Mining & Technology (Beijing) [10] and many other research groups throughout world searching for alternative glass sealants [11–16].

Recently we have proposed akermanite ($Ca_2MgSi_2O_7$)–gehlenite ($Ca_2Al_2SiO_7$) type melilite glasses within the system of CaO–MgO–Al_2O_3–SiO_2 and investigated their suitability for several functional applications [17]. Materials from this system, in particular MB-0 (in mol.% 44.01 CaO–11.02 MgO–33 SiO_2–11 Al_2O_3–0.97 La_2O_3–0 Bi_2O_3), and MB-1 (in mol.% 43.95 CaO–10.99 MgO–32.96 SiO_2–10.99 Al_2O_3–0.98 La_2O_3–0.14 Bi_2O_3), revealed to be potential candidates for SOFC seals because: (i) the CTEs could be tailored to match those of interconnect materials; (ii) an easy sealing below 1000 °C; (iii) good wetting behavior toward the interconnect materials under various atmospheric conditions; and (iv) they are Ba-free. However, sintering ability of MB-0 and MB-1 glasses was not completely satisfactory. As has also been shown in our previous studies [18], good sintering ability is crucial for a sealing glass that is applied in the powder form on the ceramic or metallic surfaces to be sealed. The poor sintering ability will result in glass-ceramic with high porosity, the path for fuel leakage, and low flexural strength. Moreover, sintering is always the final step for controlled densification and micro structural evolution.

In view of the above, the present work aims at: (i) improve the sintering ability of the sealants by changing the composition of the parent glass MB-0. The modifications made consisted on reducing the contents of glass modifiers (CaO and MgO) while increasing the amounts of network formers (SiO_2 and Al_2O_3) to obtain the CMAS composition: 38.7 CaO–9.7 MgO–12.9 Al_2O_3–38.7 SiO_2 (in mol.%); (ii) checking the suitability of the proposed glass for SOFCs sealing applications. Generally, glasses showing stability against devitrification at the SOFCs operating temperatures show crack-healing behavior above the glass softening temperature and might behave as self-healing materials. Moreover, electrical conductivity measurements also evidenced that the mobility of network-modifier cations such as calcium is about ten times faster than that of the network-forming cations [17,19–22]. Therefore, increasing the amounts of SiO_2 and Al_2O_3 at the expense of CaO and MgO appears as an interesting approach to overcome these limitations.

2. Experimental

Table 1 presents the detailed composition of the CMAS glass. High purity powders of SiO_2 (>99.5%), Al_2O_3 (Sigma Aldrich, >98%), (purity >99.5%), $CaCO_3$ and $MgCO_3$ (BDH chemicals, UK, >99%), were used. Homogeneous batch mixtures of 100 g (Table 1), obtained by ball milling were preheated at 900 °C for 1 h for decarbonization and then melted in Pt crucibles at 1590 °C for 1 h, in air. Glass in bulk form was produced by pouring the melt in preheated cylindrical bronze mold followed by annealing at temperature around T_g while glass frit was obtained by quenching of glass melt in cold water. The frit was dried and then milled in a high-speed agate mill resulting in a fine glass powder with mean particle size of $\sim$11 μm (determined by light scattering technique; Coulter LS 230, Beckman Coulter, Fullerton CA; Fraunhofer optical model). The amorphous nature of glass was confirmed by X-ray diffraction (XRD) analysis (Rigaku Geigerflex D/Max, Tokyo, Japan; C Series; Cu K_α radiation; 2θ range 10–80°; step 0.02° s^{-1}).

2.1. Density and dilatometric behavior

Archimedes' method (by immersion in diethyl phthalate) was employed to measure the apparent density of the bulk annealed glass and GCs. The obtained density values were further employed along with composition of glass to calculate the molar volume and excess molar volume.

The glass transition temperature (T_g) and softening point (T_s) of glass, and the CTE of glass and GCs were obtained by dilatometry using prismatic samples with a cross section of 4 $\times$ 5 mm (Bahr Thermo Analyze DIL 801 L, Hullhorst, Germany; heating rate

Table 1
Properties of the investigating bulk glass and glass-ceramic.

Properties	Value
CMAS-composition	35.0 CaO–6.3 MgO–21.2 Al_2O_3–37.5 SiO_2 (wt.%) 38.7 CaO–9.7 MgO–12.9 Al_2O_3–38.7 SiO_2 (mol.%)
Average particle size of glass powder, (μm)	10.96
Density of glass (g cm^{-3})	2.91 ± 0.01
V_m (cm^3 mol^{-1})	21.327 ± 0.008
V_e (cm^3 mol^{-1})	1.685 ± 0.008
T_g (°C)	732 ± 3
T_s (°C)	817 ± 3
CTE ($\times 10^{-6}$ K^{-1}) (200–500 °C)	9.7 ± 0.1
Shrinkage (%)[a]	16.93 ± 0.2
Density (g cm^{-3})[a]	2.912 ± 0.001
Bending strength (MPa)[a]	106 ± 14
Weibull characteristic strength (σ_0 MPa)[a]	108
Weibull modulus (m)[a]	7.5

[a] Glass-ceramics produced at 900 °C for 1 h.

5 K min^{-1}). The dilatometry measurements were made on a minimum of 3 specimens from each G/GC and the standard deviations for the reported CTE values are within the range $\pm 0.1 \times 10^{-6}$ K^{-1}.

2.2. Structural characterization of glasses

Infrared spectrum of glass was obtained using an Infrared Fourier spectrometer (FT-IR, model Mattson Galaxy S7000, USA). For this purpose, the glass powder was mixed with KBr in the proportion of 1/150 (by weight) and pressed into a pellet using a hand press. 64 scans for background and 64 scans per sample were made with signal gain 1. The resolution was 4 cm^{-1}.

^{29}Si magic angle spinning (MAS) nuclear magnetic resonance (NMR) spectrum was recorded on a Bruker ASX 400 spectrometer operating at 79.52 MHz (9.4 T) using a 7 mm probe at a spinning rate of 5 kHz. The pulse length was 2 μs and 60 s delay time was used. Kaolinite was used as the chemical shift reference. ^{27}Al MAS-NMR spectrum was recorded in the same instrument but operating at 104.28 MHz (9.4 T) using a 4 mm probe at a spinning rate of 15 kHz. The pulse length of 0.6 μs and a delay time of 4 s were used. $Al(NO_3)_3$ was used as the chemical shift reference.

2.3. Sintering behavior and thermal analysis of glasses

The sintering behavior of the glass powder was investigated using a side-view hot stage microscope (HSM) EM 201 equipped with image analysis system and 1750/15 Leica electrical furnace. The cylindrical shaped sample with height and diameter of ~3 mm was prepared by cold-pressing the glass powder and placed on a 10 × 15 × 1 mm alumina (~99.5 wt.% Al_2O_3) support. The temperature was measured with a Pt/Rh (6/30) thermocouple contacted under the alumina support. The microscope projects the image of the sample through a quartz window and onto the recording device. The computerized image analysis system automatically records and analyses the geometry changes of the sample during heating. The image analyzer takes into account the thermal expansion of the alumina substrate while measuring the height of the sample during firing, with the base as a reference. The HSM software calculates the percentage of decrease in height, width and area of the sample images. The measurements were conducted in air with a heating rate of 5 K min^{-1}. The temperatures corresponding to the characteristic viscosity points were obtained from the photographs taken during the hot-stage microscopy experiment following Scholze's definition [23,24].

The differential thermal analysis (DTA, Setaram Labsys, Setaram Instrumentation, Caluire, France) of glass powder weighing 50 mg was carried out in air from room temperature to 1200 °C at 5 K min^{-1} in an alumina crucible using α-alumina powder as reference material. The standard deviation values reported for the crystallization onset temperature (T_c) and peak temperature of crystallization (T_p) as obtained from DTA are within the range of ±3 °C.

2.4. Crystalline phase evolution in glass-ceramics

Rectangular bars with dimensions of 4 × 5 × 50 mm were prepared by uniaxial pressing (80 MPa). The linear shrinkage during sintering was calculated from the difference in the dimensions between the green and the sintered bars. Archimedes' method (i.e., immersion in diethyl phthalate) was employed to measure the apparent density of the sintered GCs. The mechanical property was evaluated by measuring the three-point bending strength of rectified parallelepiped bars of sintered GCs (Shimadzu Autograph AG 25 TA, Columbia, MD; 0.5 mm min^{-1} displacement). The mean values and the standard deviations (SD) presented for, shrinkage, density and bending strength have been obtained from at least 10 different samples. The powder compacts were sintered at 900 °C for 1 h and under isothermal conditions for 300 h at 850 °C. A slow heating rate of 5 K min^{-1} was maintained in order to prevent deformation of the samples. The amorphous nature of glasses and the quantitative analysis of crystalline phases in the GCs (crushed to particle size <45 mm) was made by XRD analysis using a conventional Bragg–Brentano diffractometer (Philips PW 3710, Eindhoven, The Netherlands) with Ni-filtered Cu–K radiation. The quantitative phase analysis of GCs was made by combined Rietveld-R.I.R (reference intensity ratio) method. 10 wt.% corundum (NIST SRM 676a) was added to all the GC samples as an internal standard. The mixtures, ground in an agate mortar, were side loaded in aluminum flat holder in order to minimize the preferred orientation problems. Data were recorded in 2θ angle range 15–115°; step 0.02° s^{-1}. The phase fractions extracted by Rietveld-R.I.R refinements, using GSAS software and EXPGUI as graphical interface, were rescaled on the basis of the absolute weight of corundum originally added to their mixtures as an internal standard, and therefore, internally renormalized. The background was successfully fitted with a Chebyshev function with a variable number of coefficients depending on its complexity. The peak profiles were modeled using a pseudo-Voigt function with one Gaussian and one Lorentzian coefficient. Lattice constants, phase fractions, and coefficients corresponding to sample displacement and asymmetry were also refined.

2.5. Weibull statistics

The bending strength of the GCs sintered at 900 °C for 1 h was measured (Shimadzu Autograph AG 25 TA, Columbia, MD; 0.5 mm min^{-1} displacement) and the mechanical reliability was tested by applying the well-known Weibull statistics to the experimental data [25]. According to Weibull statistics, the increasing probability of failure (F) for a brittle material can be expressed by $F = 1 - \exp(-\sigma/\sigma_0)^m$, where F is the failure probability for an applied stress (σ), σ_0 is a normalizing parameter known as Weibull characteristic strength, and m is the Weibull modulus. Here, the Weibull modulus m is a measure of the degree of strength data dispersion. While applying the Weibull statistics to the mechanical strength data help were taken from [26].

2.6. Joining behavior and chemical interactions between electrolyte/seal and interconnect/seal diffusion couples

To investigate the adhesion and chemical interactions of the glass with SOFC components, wetting experiments between glass (powder) – solid electrolyte (8YSZ) and glass-interconnect (Sanergy HT) were carried out. A 40 wt.% suspension of the glass powder was prepared in a 5 vol.% solution of polyvinyl alcohol (PVA) in water and deposited onto the YSZ electrolyte and Sanergy HT substrates by slurry coating. The diffusion couples were heated to 900 °C with a relatively slow β of 2 K min^{-1} and kept at that temperature for 1 h. Heat treatment was performed without applying any dead load.

2.7. SEM–EDS analysis

Microstructural observations on polished surfaces of the sintered glass powder compacts (chemically etched by immersion in 2 vol.% HF solution for a duration of 2 min) and micrograph of fractured surface after the mechanical strength measurements were made by scanning electron microscopy (SEM; SU-70, Hitachi) with energy dispersive spectroscopy (EDS; Bruker Quantax, Germany) to study the distribution of elements in the crystals and along the glass-ceramics-interconnect diffusion couples.

3. Results

3.1. Glass forming ability and glass properties

The experimental glass composition was prone for easy casting at 1590 °C for 1 h resulting in homogeneous and transparent bulk glass and glass frit quenched in water. The bulk glass in the form of rods was annealed at a temperature around T_g for 1 h; its amorphous nature was confirmed by XRD analysis. The glass frit was milled to a mean particle size of ~11 μm. The density, molar volume, and excess molar volume of the glass were measured as 2.90 g cm^{-3}, 21.33 cm^3 mol^{-1} and 1.68 cm^3 mol^{-1} respectively (Table 1). The values of the glass transition temperature (T_g), softening temperature (T_s) and CTE are presented in Table 1.

3.2. Structure of glass

The room temperature FTIR transmittance spectra of the investigated glass is shown in Fig. 1. The glass exhibits three broad transmittance bands in the region of 300–1400 cm^{-1}. This lack of sharp feature is an indicative of general disorder in the silicate network mainly due to the wide distribution of Q^n units (polymerization in the glass structure, where n denotes the number of bridging oxygens) occurring in the glasses. The most intense broad band in the 800–1200 cm^{-1} region indicates the stretching vibrations of Si–O–Si linkages in the SiO_4 tetrahedron unit. The appearance of high intensity broad band at 953 cm^{-1} due to the nonbridging Si–O terminal stretching vibrations, suggest that Q^2 units are highly localized. The band in the 300–600 cm^{-1} region corresponds to bending vibrations of Si–O–Si and Si–O–Al linkages [27]. With respect to the aluminum coordination in glass structure, the presence of transmittance band from medium to strong intensity in the 600–750 cm^{-1} region with the center of gravity at ~694 cm^{-1} is a typical feature of stretching vibration of the Al–O bond with aluminum ions in Al four coordination [28,29].

The broad ^{29}Si MAS-NMR spectrum of the glass (Fig. 2(a)) implies toward a wide distribution of Q^n (Si) units in the glass structure with peak centered at −78 ppm (Q^2 units). The ^{27}Al NMR spectrum of the glass (Fig. 2(b)) manifests signal-broadening from paramagnetic-driven relaxation process and depict the dominance of tetrahedral-coordinated aluminum with its maxima at ca. 56 ppm. It is well-known that chemical shift in ^{27}Al NMR spectrum is strongly affected by the local coordination of aluminum ions. Though we could not confirm the presence of ^{V}Al and ^{VI}Al species in this glass with maxima at ~30 ppm and 0 ppm, respectively the presence of ^{V}Al species cannot be neglected in this glass as these species has been reported to exist in a variety of alkali/alkaline-earth aluminosilicate glasses [30]. The ^{IV}Al resonance in the CMAS glass has typical asymmetric form with tail extending toward lower frequency resulting from the distributions in quadrupolar coupling constants.

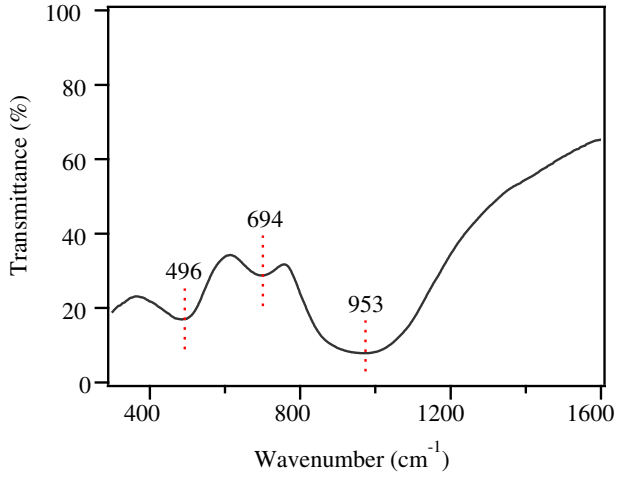

Fig. 1. FTIR spectra of the investigated glass powder.

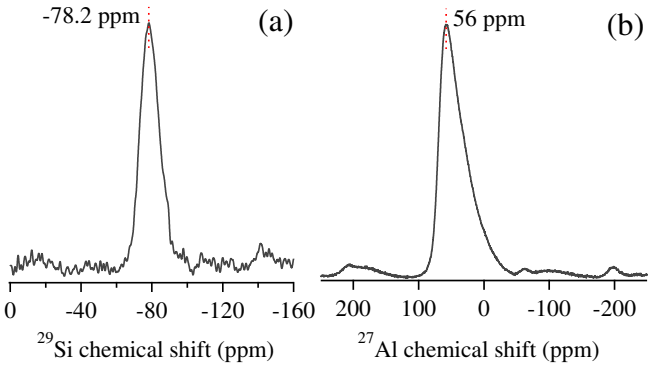

Fig. 2. (a) ^{29}Si MAS-NMR spectrum, and (b) ^{27}Al MAS-NMR spectrum of the investigated glass.

3.3. Sintering and crystallization

DTA and HSM measurements under the same heating conditions were utilized to observe sintering and devitrification behavior in the present glass system. Fig. 3(a) represents the variations in the relative area of glass powder compact and heat flow with respect to temperature as obtained from HSM and DTA, respectively at the heating rate of 5 K min^{-1}. From Fig. 3(a), it can be seen that the onset temperature of crystallization (T_c) of the present glass, occurs after the final sintering stage, making sintering and crystallization independent processes. This contrasts with the MB-0 composition reported before [17] for which T_c occurred before maximum density has been reached, and the crystallization process indicated before complete densification tended to hinder further sintering.

Table 2 summarizes the data obtained from HSM at T_{MS} (Fig. 3(a)), including: temperature of first shrinkage (T_{FS}; $\log \eta = 9.1 \pm 0.1$; η is viscosity in dPa s); temperature for maximum shrinkage (T_{MS}; $\log \eta = 7.8 \pm 0.1$); temperature for deformation (T_D; $\log \eta = 6.3 \pm 0.1$); temperature for haff-ball (T_{HB}; $\log \eta = 4.1 \pm 0.1$); temperature for flow (T_F; $\log \eta = 3.4 \pm 0.1$); along with temperature for onset of crystallization (T_c), peak temperature of crystallization (T_p) as received from DTA [24]. The following observations can be made from Table 2 and the DTA and HSM measurements for the investigated glass:

(i) The first sintering stage was observed to start at $T_{FS} = 819$ °C;
(ii) The CMAS glass exhibits a single sintering stage behavior with the maximum densification ($T_{MS} = 895$ °C) being achieved before the crystallization onset temperature (T_c), i.e., $T_{MS} < T_c$ demonstrating that sintering precedes crystallization and, therefore, well sintered and mechanically strong glass powder compacts should be expected.
(iii) The sintering ability parameter S_c ($=T_c - T_{MS}$) value (22) calculated for the present CMAS glass is significantly higher than that found for the MB-0 glass (−5) [17]. Higher S_c values mean delayed nucleation and crystallization events, thus a wider processing window for a glass composition to attain maximum densification. These features confer to the present glass good suitability as sealant for SOFCs.

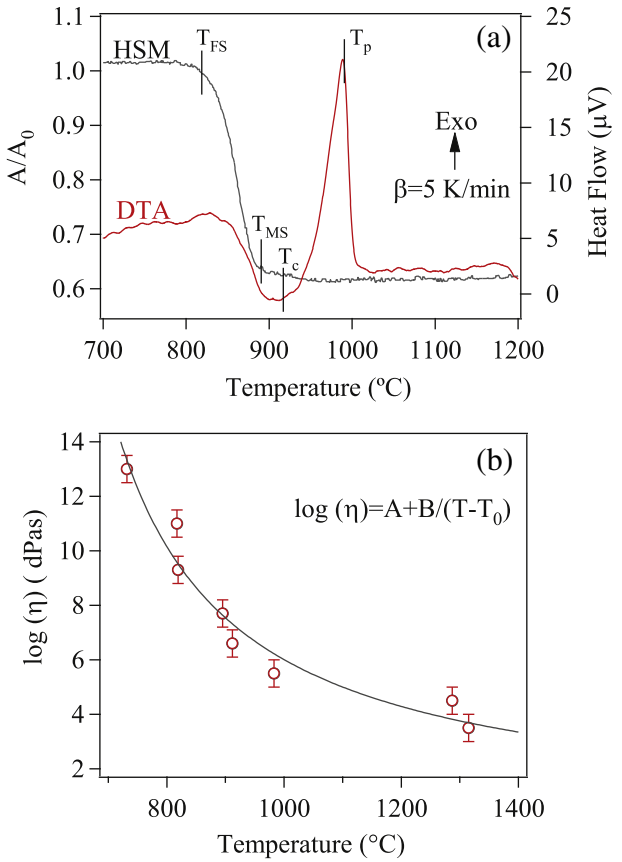

Fig. 3. (a) HSM and DTA curves on the temperature scale (b) VFT equation ($\log \eta = A + B/(T - T_0)$) fitted to the viscosity points obtained from dilatometric and HSM measurements.

(iv) The DTA thermograph exhibits a single crystallization exothermic curve, meaning that the resulting glass-ceramic consists of single or of more than one crystalline phase but precipitated simultaneously.

(v) The geometrical changes of the glass with temperature depicted in the photomicrographs of Fig. 4 reveal a deformation temperature (temperature at which the first signs of softening are visually observed, generally shown by the disappearance or rounding of the small protrusions at the edges of the sample) at 912 °C, and a sphere formation temperatures at 983 °C, whereas half-ball and flow temperatures were obtained at 1287 °C and 1315 °C, respectively. However, the significant difference ($T_c - T_g = 185$ °C) means a large ability of the CMAS glass to flow, accommodate mechanical stresses arising from any CTE mismatch, and to act as self-healing material.

Table 2
Thermal parameters of the glass obtained from DTA and HSM at $\beta = 5$ K min^{-1}.

Thermal parameter	Temperature (°C)
T_{FS} ±5	819
T_{MS} ±5	895
T_c ±5	917
T_D ±5	912
T_p ±2	988
T_s ±5	983
T_{HB} ±5	1287
T_{FS} ±5	1315
S_c (=$T_c - T_{MS}$)	22
VFT equation constants	$A = 1.00$ (kPa s); $B = 1973$ (kPa s °C); $T_0 = 576.54$ (°C)

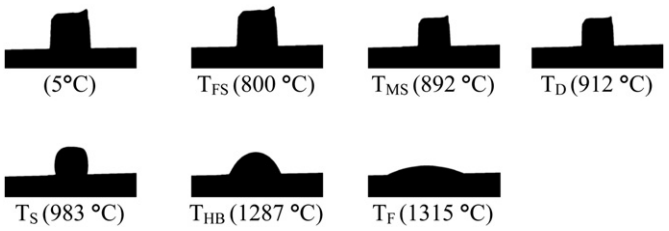

Fig. 4. HSM images of glass on alumina substrates at various stages of the heating cycle.

(vi) Fig. 3(b) represents the viscosity curves for the present investigated glass measured by least squares fitting of HSM and dilatometric characteristic points using the Vogel–Fulcher–Tammann (VFT) relation $\log \eta = A + B/(T - T_0)$ [23,24] where η is the viscosity and T the temperature. The coefficients A, B and T_0 deduced from the fitting are reported in Table 2. The calculated reduced viscosity of glass at 900 °C from the VFT equation was close to $\sim 10^{7.1}$ dPa s, suitable for sealant applications [24].

(vii) The value of the ratio of the final area/initial area of the glass powder compact, $A/A_0 = 0.63$ implies toward good densification (95–98%) [31].

All of these properties are of high relevance and should be present in good sealing materials for applications in SOFCs.

3.4. Crystalline phase evolution and thermal stability

In accordance with the DTA and HSM results, full dense glass powder compacts were obtained after sintering at 900 °C for 1 h, as confirmed by the SEM images of GCs presented in Fig. 5. There was no evidence of deformation or open porosity as also confirmed by the density, shrinkage and bending strength data (Table 1). Fig. 6 presents X-ray diffractograms of the sintered glass powder compacts at 900 °C for 1 h and of the compacts sintered at 850 °C for 300 h depicting the evolution of crystalline phases. The samples were still amorphous after heat treatment at 800 °C for 1 h (not shown). Table 3 presents the quantitative analysis of the crystalline phases present in all the investigated GCs as obtained from XRD analysis adjoined with Rietveld-R.I.R technique. Fig. 7 shows the measured XRD pattern fits for GCs sintered at 850 °C for 300 h, by using the GSAS EXPGUI software. The calculated diagrams are based on crystallographic structure models, which also take into account specific instrument and sample effects. The parameters of this model have been refined simultaneously using least-squares methods in order to obtain the best fit to all measured data. By least-squares refinement, a so-called figure-of-merit function R has been defined, which describes the residual (agreement) between observed and calculated data [32]. It is noteworthy that many different statistical R factors have been proposed for judging the quality of a Rietveld refinement. The R factors show the mean deviation in accordance with the model used in percent. The "profile R-factor", R_p, and "weighted profile R-factor", R_{wp}, for all the refinements are presented in Table 3. The values of R_{wp} as obtained in the present investigation are well within the limits of experimental accuracy. The difference plot in Fig. 7 does not show any significant misfits. The differences between the main peaks of akermanite–gehlenite solid solution and anorthite are caused by adjustment difficulties based on the crystallinity of the phases.

Akermanite–gehlenite ($Ca_2Mg_{0.35}Al_{1.3}Si_{1.35}O_7$) (16.6 wt.%) and merwinite (5.2 wt.%) were the two crystalline phases formed upon

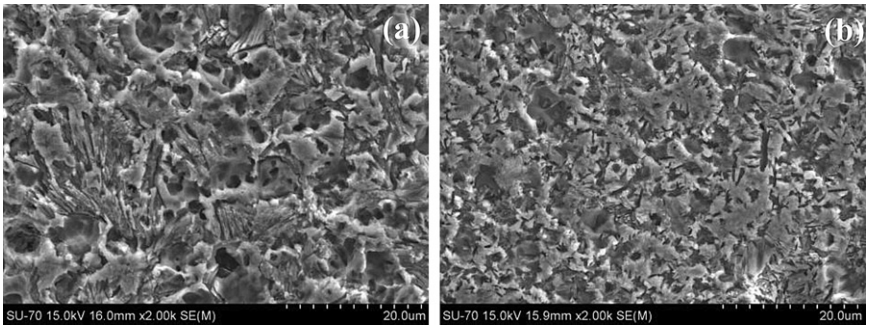

Fig. 5. Microstructure (revealed via SEM imaging after chemical etching of polished surfaces with 2 vol.% HF solution) of the GCs heat treated at (a) 900 °C for 1 h and (b) 850 °C for 300 h.

sintering at 900 °C for 1 h, summing up a total of about 22 wt.% crystalline material and 78 wt.% of amorphous glass. The high amount of residual glassy phase in the investigated glass makes as a potential candidate for self-healing glass-ceramic seals. However, after the prolonged heat treatment (850 °C, 300 h) the amorphous quantity was reduced significantly to ~19 wt.%, forming akermanite–gehlenite solid solution (~59 wt.%) as the major phase followed by anorthite (~22 wt.%) as the second crystalline phase. The standard diffraction patterns of akermanite–gehlenite (ICDD: 76–7527), merwinite ($Ca_3Mg(SiO_4)_2$; ICDD: 35–0591), and anorthite ($CaAl_2Si_2O_8$; ICDD: 41–1486) were also included in Fig. 5 for comparison purposes.

3.5. Glass-ceramic properties

Usually, glass powders in which crystallization precedes sintering result in small shrinkage, porous and mechanically weak GCs. In the present work, the high values of shrinkage (~17%), density (2.91 g cm^{-3}, equal to that of bulk glass) and mechanical strength (106 MPa) confirm the good densification of glass powder compacts.

Even small differences in thermal expansion ($\Delta\alpha \sim 10^{-6}\ K^{-1}$) of the materials and components comprising the planar SOFC arrangement might generate residual stresses in all stack. The residual and operation stresses endanger the mechanical integrity of the sealant, which ultimately might terminate the stack lifetime. In order to characterize mechanical strength of CMAS seal, the two-parameter Weibull strength distribution for the CMAS glass-ceramic sintered at 900 °C for 1 h is presented in Fig. 8(a). In mechanical failure of a brittle material, the Weibull modulus is related to the shape, size, and distribution of strength-controlling flaws. A large Weibull modulus represents a less degree of scattering in strength data, which was caused by a smaller range of distribution in flaw size and shape. The relatively high Weibull modulus (m ~7–8) means good mechanical reliability for the sealants. The Weibull characteristics strength (σ_0 = 108 MPa) is higher than those reported for G-18 glass (51 MPa) [33], G-18 glass BNNT composites (92 MPa) [33], and GC-9 glass (41–78 MPa) [12]. Fig. 8(b) shows the typical fracture surface of a bending strength tested specimen. In general, when CTE values of components are higher than that for glass seal, tensile/compressive stress will occur at the interface of the glass/glass-ceramic sealant and components upon heating/cooling cycles. Thus, a close match of the CTEs of all components is essential for the mechanical integrity and hermeticity of the join between metal–ceramic or ceramic–ceramic components of SOFC [5–7]. The CTE values of the GCs (GC) sintered at 900 °C for 1 h and at 850 °C for 300 h are presented in Table 3.

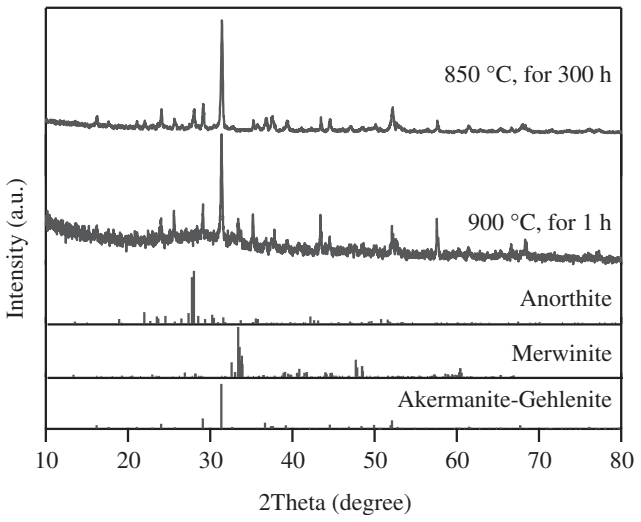

Fig. 6. X-ray diffractograms of glass-powder compacts sintered at various conditions.

3.6. Interaction studies

Figs. 9(a) and 10(a) show the SEM images of the interfaces between Sanergy HT/GC and 8YSZ/GC, respectively, formed by heat treating the pair joints (Sanergy HT/CMAS and 8YSZ/CMAS) at 900 °C for 1 h in air. Figs. 9(b)–(d) and 10(b)–(d) show the EDS elemental mapping of the relevant elements existing at the interface after heat treatment at 900 °C for 1 h in air. CMAS GC seal bonded well to the Sanergy HT metallic interconnects and 8YSZ ceramic components of SOFCs, and the investigated interfaces showed homogeneous microstructures over their entire cross-sections of the joint. The analysis of element mapping and

Table 3
Rietveld R.I.R., and CTE (200–700 °C) results for the GCs sintered under different conditions.

	900 °C, 1 h	850 °C, 300 h
Akermanite–gehlenite solid solution $Ca_2Mg_{0.35}Al_{1.3}Si_{1.35}O_7$	16.57	58.65
Merwinite, $Ca_3MgSi_2O_8$	5.19	–
Anorthite, $CaAl_2Si_2O_8$	–	22.02
Glass	78.24	19.33
χ^2	1.243	1.594
R_F^2	0.348	0.204
W_{RP}	0.156	0.179
R_p	0.118	0.135
CTE ($\times 10^{-6}\ K^{-1}$)	10.1	10.0

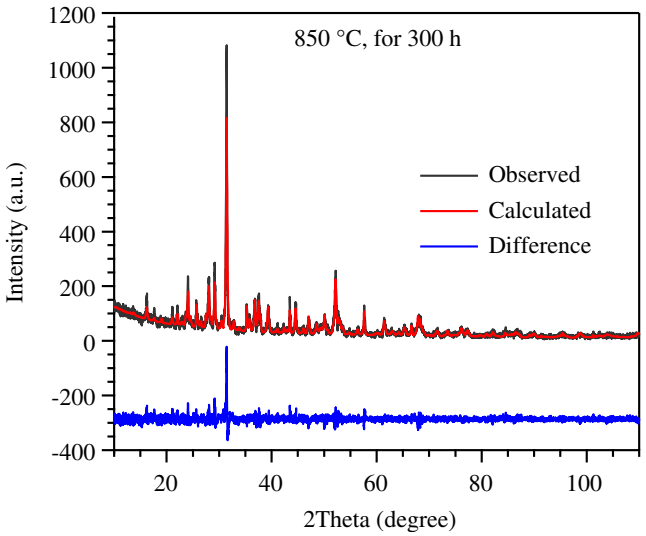

Fig. 7. Observed, calculated, and difference curve from the Rietveld refinement of the glass-ceramic heat treated at 850 °C for 300 h.

elemental line profiles (inserted plots in Figs. 9(a) and 10(a)) confirmed formation of a smooth interface between investigated glass-ceramic seal and SOFCs Sanergy HT metallic plate and 8YSZ ceramic plate. However, a thin reaction zone of Mn and Cr-rich oxide layer was formed at the steel side of the interface, indicating the formation of manganese–chromium spinal. Further, no negative influence with respect to adhesion and cracking at the interface was observed with the CMAS GC sealant.

4. Discussion

A seal glass should be sintered well in order to avoid the formation of voids and reduce the amount and size of strength flaw populations that limit the mechanical strength and the reliability of the resultant GC. Gehlenite and akermanite belong to melilite group of silicates and form continuous solid solutions. Due to the high content and the mobility of alkaline-earth ions in these glasses intermediate crystalline phases are forming and hindering the complete densification in the resultant GCs. In our previous study we attempted controlling the mobility of CaO and avoiding the formation of meta-stable crystalline phases by adding to the glass composition different amounts of low melting point Bi_2O_3. Enhanced sintering was only observed in the presence of a small amount of Bi_2O_3. The expected decrease in viscosity of the melts facilitated the diffusion of the dominating alkaline-earth ions, hindering densification [17]. In the present report the alkaline-earth ions were partially replaced by network forming ions.

It can be seen that the CTE (200–500 °C) of the glass was reduced from 10.9 (MB-0) to 9.7×10^{-6} K^{-1} due to rearrangements in the glass network structure as the thermal expansion behavior of a glass is controlled by its network bonding strength. Concerning the glass structure, with the decrease in content of alkaline-earths the major silicate band in the region 800–1200 cm^{-1} and the tetrahedral coordination band in the region 600–750 cm^{-1} shifted toward the higher wavenumber directions, evidencing the polymerization of the silicate network. This is well correlated with the results of Kuryaeva [34], according to whom, alkali/alkaline-earth cations either compensate for the negative charge or form non-bridging bonds that partially destroy the structural network. MAS-NMR ^{27}Al spectrum of glass presents the dominance of tetrahedral coordinated aluminum with its maxima at ~56 ppm, confirming FTIR results.

With respect to silicon coordination in glasses, the predominant feature that determines a first approximation of the isotropic ^{29}Si chemical shifts is the number of Si and Al atoms attached to the SiO_4 unit being considered in solid aluminosilicates with increasing polymerization of Q^n building units, i.e., shielding of the central Si atom increases in the sequence $Q^0 < Q^1 < Q^2 < Q^3 < Q^4$. According to Murdoch et al., [35] an increase in the number of Al next–nearest neighbors deshields the Si nucleus, on average, by 5.5 ppm Al^{-1} neighbor. Also, the presence of several distinct modifier ions and, particularly, additional network formers result in featureless NMR spectra, due to the dependence of the position of other cations and neighboring oxygen species. The ^{29}Si peak position for the investigated glass lies at ~−78.2 ppm may represent highly polymerized species with many Al neighbors or less polymerized units with low or no Al neighbors. In the present scenario, the latter option with less polymerized silicate units (a mixture of $Q^2 + Q^3$ units) and low or no Al neighbors seem to be more feasible because of high alkaline-earth content in glasses in comparison to Al_2O_3.

In the present study, sintering was initiated at the same temperature (T_{FS}) as reported for MB-0 glass. On the other hand, maximum densification, onset crystallization and peak crystallization occurred at higher temperatures compared to MB-0 glass. In general, maximum densification is reached when larger pores (pores formed from cavities among larger particles) have disappeared due to viscous flow that reduces their radii with time. This region of sintering kinetics may be described by the Mackenzie–Shuttle worth model of sintering [36]. However, the study of the viscosity of melts in the $CaO–Al_2O_3–SiO_2$ system

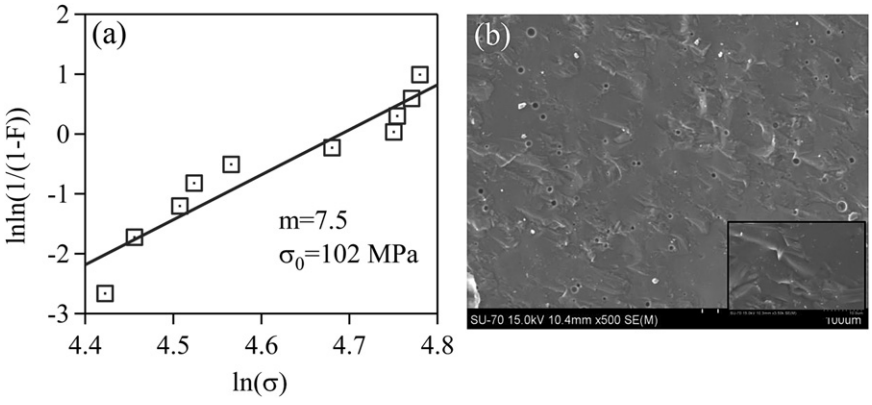

Fig. 8. (a) Weibull distribution of flexural strength, and (b) typical fracture surface of a tested specimen showing fracture origin and pores for the GC sintered at 900 °C for 1 h.

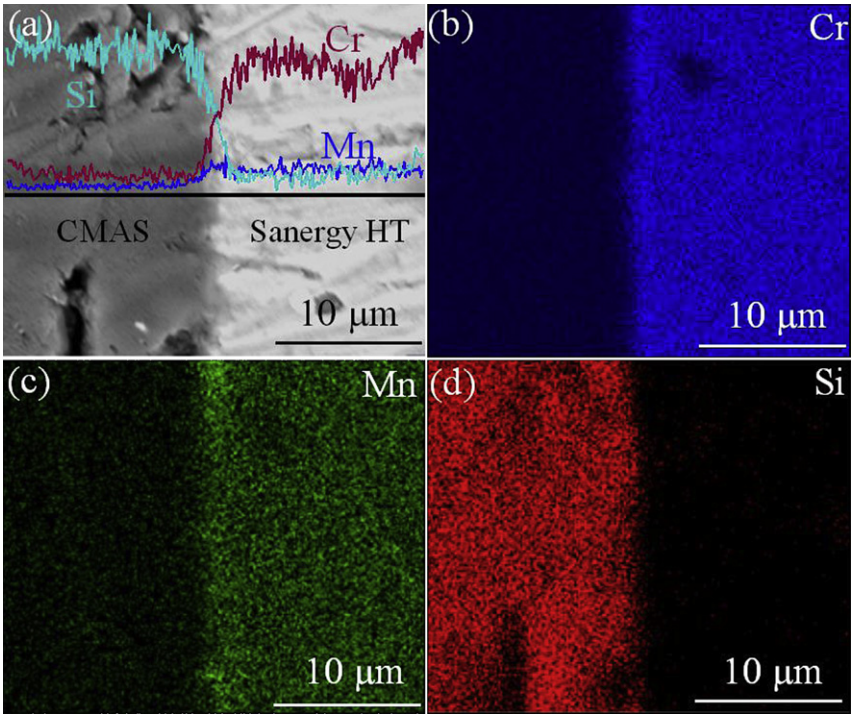

Fig. 9. (a) SEM images of the polished interfaces across the joint GC-CMAS/SANERGY HT heat treated at 900 °C for 1 h in air atmosphere. EDS element mapping of the (b) Cr (c) Mn and (d) Si at the interface of the joint GC-CMAS/SANERGY HT. Inserted plots in Fig. 9a shows EDS line scan for Cr, Mn and Si across the joint.

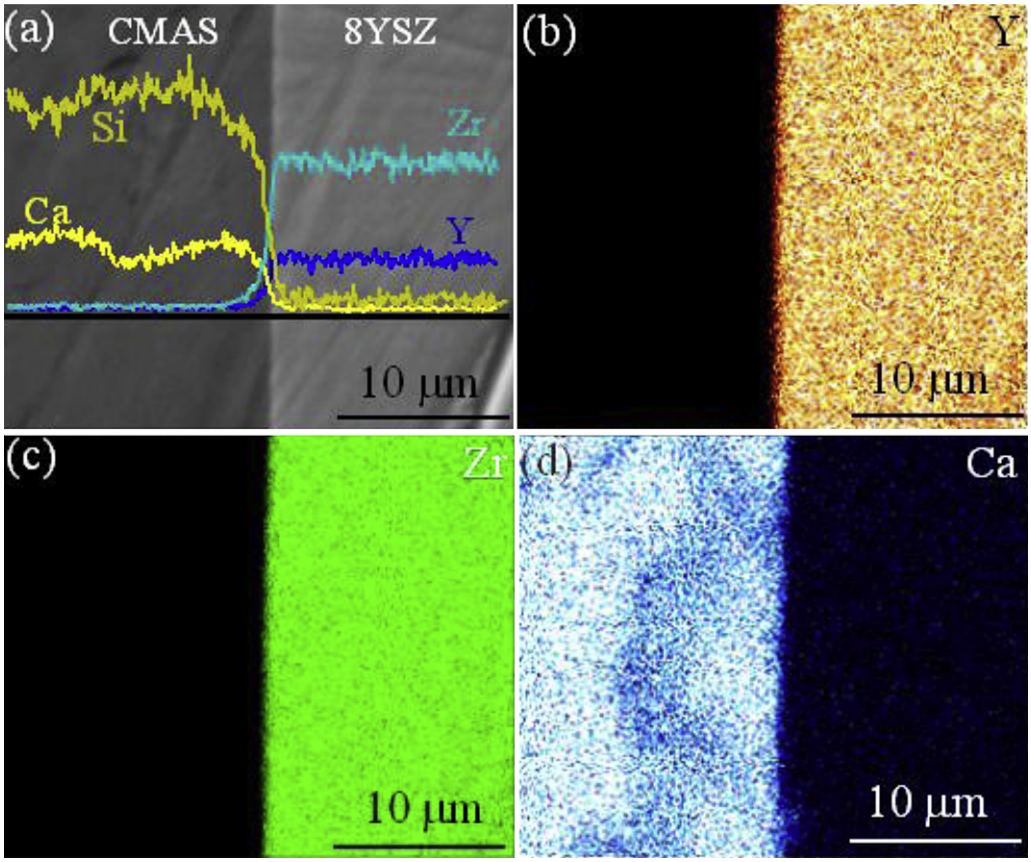

Fig. 10. (a) SEM images of the polished interfaces across the joint GC-CMAS/SANERGY HT heat treated at 900 °C for 1 h in air atmosphere. EDS element mapping of the (b) Cr (c) Mn and (d) Si at the interface of the joint GC-CMAS/SANERGY HT. Inserted plots in Fig. 10a shows EDS line scan for Y, Zr, Si and Ca across the joint.

[37] has demonstrated that, in calcium-containing melts with a ratio Ca/2Al >1, the viscosity increases with decreasing the Ca/(Ca + 2Al) ratio (1.5 for CMAS and 2 for MB-0 glass). It has been further reported that Al_2O_3 affects the diffusion mechanism at the initial stages of sintering, causing a decrease of activation energy of diffusion [38]. This might explain why the maximum densification and crystal growth mechanisms were shifted to higher temperature and enhanced the sintering ability ($S_c = 22$). It is worthy to note that the half-ball and flow behavior could not be observed by HSM for the MB–0 glass even up to 1400 °C, contrarily to CMAS glass exhibited these features at the 1287, and 1312 °C, respectively (Fig. 5). Therefore, the changes performed in the parent MB-0 composition caused lower viscosity and improved flow behavior of the glass at the sintering temperature range. It is well-known that the transport properties of silicate melts are strongly dependent on minor changes in composition. For example, when a silica–rich melt is mixed with just several weight percent of another oxide (e.g., MgO, Na_2O, etc.) the melt viscosity can be reduced by several orders of magnitude [39].

A smooth variation of viscosity with temperature (Fig. 3(b)), i.e., low fragility, is one of the most important conditions for obtaining a good seal. Although in some cases the parameter *B* of the VFT equation is related to the activation energy of the viscous flow, it should be pointed out that three constants in the VFT equation have no physical significance and are mainly used to interpolate between the viscosity values. The viscosity of the sealing glass must be low enough ($\sim 10^6$–10^8 dPa s) at a maximum temperature of 900 °C to enable spreading and bonding to the other SOFC components, and undergo an important variation in viscosity on a narrow temperature range. Fig. 3(b) shows that viscosity varies between 10^6 and 10^9 dPa s within the sealing range (800–900 °C). Thus, good requirements for sealing are accomplished for this glass.

Table 3 shows that the amount of crystalline akermanite–gehlenite phase increased significantly under prolonged heat treatment. However, as crystallization proceeds toward thermodynamic equilibrium, gehlenite reacts partially or totally with silica to form anorthite ($CaAl_2Si_2O_8$) so that the remaining melilite becomes gradually poor in the aluminum component [40]. Thus, further structural characterizations and more experiments are needed to discuss more about the formation and stability of anorthite crystalline phase after longer heat treatment such as 1000 h.

The conchoidal type fracture surfaces of specimens used in bending strength tests (Fig. 8(b)), typical of glassy materials, show that failure origins were from either surface flaws with their sizes ranging approximately from 5 to 100 μm or from volume spherical pores (1–5 μm) derived from bubbles entrapped in the coating glass slurry. As revealed from X-ray quantitative analysis, the samples sintered for 1 h at 900 °C consist of about 78% of glassy phase justifying the conchoidal morphology of the fracture surface.

Mechanical properties of glass-ceramic materials generally depend on the mechanical properties of the main crystalline phases, which occupy a portion of the volume in material [12]. In this regard, the high crystalline fraction (~78 wt.%) of GC sintered at 850 °C for 300 h is likely to enhance the mechanical strength under the SOFC operating conditions and thermal cycling. This hypothesis is under investigation and the pertaining data will be report in a forth coming article along with the mechanical strength measurements at higher temperature. A large Weibull modulus, called the shape factor *m*, relates to the uniformity of the distribution of flaws in a brittle material: a high value of *m* implies a highly uniform distribution of defect sizes and therefore a low level of variability of seal strengths. Conversely, a low value of *m* implies highly variable flaw sizes and a large spread of measured strengths. The large Weibull modulus obtained (low degree of scattering in strength data) for CMAS glass points out to good reliability of the sealing process.

The small variation (0.1×10^{-6} K^{-1}) observed in the CTE values for GCs subjected to different heat treatments (900 °C, 1 h, or 900 °C for 1 h + 850 °C, 300 h) (Table 3), means excellent stability of this important thermal parameter. Moreover, the CTE values ($\sim 10.1 \times 10^{-6}$ K^{-1}) of GCs sintered under various conditions are in good agreement with those of ceramic electrolyte, 8YSZ ($\sim 10 \times 10^{-6}$ K^{-1}) and metallic interconnect, Sanergy HT ($\sim 11 \times 10^{-6}$ K^{-1}) [15,16], considering that differences between the CTE of SOFC components until 1×10^{-6} K^{-1} can easily be tolerated. The mechanical strength and CTE value results confirm the suitability of the CMAS glass composition for joining applications in SOFC. Regarding the chemical interactions of seals with interconnect, it is known that GCs generally show higher chemical stability than the glasses. Indeed, no appreciable diffusion of elements from the investigated GCs toward the Sanergy HT and *vice versa* was detected. The formation of an inter diffusion Cr–Mn-spinel layer of about 2 μm thickness (Fig. 9), between the CMAS seal glass and interconnect is within the acceptable applicability limit [41]. However, the formation of uniform Cr–Mn-spinel layer instead of single Cr-layer one ensures low chromium vaporization during operation under SOFC atmosphere conditions. The formation of a very thin (~1 μm) Cr–Mn-spinel layer can be avoided by pre-oxidation of interconnect or by using protective coatings [42].

5. Conclusions

The data presented and discussed along this manuscript enable drawing the following conclusions:

1. Slight adjustment of melilie glass composition improved the network connectivity and decreased the CTE of the glass.
2. Single stage maximum shrinkage behavior was recorded for the proposed glass. The sintering ability parameter S_c ($=T_c - T_{MS}$) of the CMAS glass was significantly increased from −5 to 22. The good sintering ability of CMAS glass enabled to achieve good levels of flexural strength and reliability.
3. The thermal and chemical stability of CMAS glass at 850 °C for 300 h satisfies most requirements to the sealants for planar SOFCs. However, further experimentation at prolonged heat treatment (till 1000 h at 850–900 °C) is needed to asses evaluation of anorthite phase and its influence on thermal parameters of GC.

Acknowledgment

This study was financially supported by the University of Aveiro, CICECO, and FCT, Portugal (PTDC/CTM–CER/114209/2009).

References

[1] E.D. Wachsman, C.A. Marlowe, K.T. Lee, Energy Environ. Sci. 5 (2012) 5498–5509.
[2] J.C. Ruiz-Morales, D. Marrero-Lopez, J. Canales-Vazquez, J.T.S. Irvine, RSC Adv. 1 (2011) 1403–1414.
[3] F. Bruijn, Green Chem. 7 (2005) 132–150.
[4] R.M. Ormerod, Chem. Soc. Rev. 32 (2003) 17–28.
[5] J.W. Fergus, J. Power Sources 147 (2005) 46–57.
[6] M.K. Mahapatra, K. Lu, J. Power Sources 195 (2010) 7129–7139.
[7] I.W. Donald, L.A. Gerrard, P.M. Mallinson, B.L. Metcalfe, L.A. Gerrard, P.M. Mallinson, J.A. Fernie, J. Mater. Sci. 46 (2011) 1975–2000.
[8] E.V. Stephens, J.S. Vetrano, B.J. Koeppel, J. Power Sources 193 (2009) 625–631.
[9] M.K. Mahapatra, K. Lu, Fuel Cells 11 (2011) 436–444.
[10] J.J. Tong, M.F. Han, S.C. Singhal, Y. Gong, J. Non-Cryst. Solids 358 (2012) 1038–1043.
[11] F. Smeacetto, A. Chrysanthou, M. Salvo, T. Moskalewicz, F. D'Herin Bytner, L.C. Ajitdoss, M. Ferraris, Int. J. Hydrogen Energy 36 (2011) 11895–11903.
[12] H.-T. Chang, C.-K. Lin, C.-K. Liu, S.-H. Wu, J. Power Sources 196 (2011) 3583–3591.
[13] W.N. Liu, X. Sun, M.A. Khaleel, J. Power Sources 196 (2011) 1750–1761.

[14] A. Goel, D.U. Tulyaganov, V.V. Kharton, A.A. Yaremchenko, J.M.F. Ferreira, J. Power Sources 195 (2010) 522–526.
[15] S.M. Gross, D. Federmann, J. Remmel, M. Pap, J. Power Sources 196 (2011) 7338–7342.
[16] M.J. Pascual, A. Guillet, A. Durán, J. Power Sources 169 (2007) 40–46.
[17] A.A. Reddy, D.U. Tulyagnov, S. Kapoor, A. Goel, M.J. Pascual, V.V. Kharton, J.M.F. Ferreira, RSC Adv. 2 (2012) 10955–10967.
[18] A. Goel, A.A. Reddy, M.J. Pascual, L. Gremillard, A. Malchere, J.M.F. Ferreira, J. Mater. Chem. 22 (2012) 10042–10054.
[19] J.F. Stebbins, S. Sen, I. Farnan, Am. Mineral. 80 (1995) 861–864.
[20] M. Roskosz, J. Gillot, F. Capet, P. Roussel, H. Leroux, Astrophys. J. 707 (2009) L174–L178.
[21] I. Farnan, J.F. Stebbins, Science 265 (1994) 1206–1209.
[22] K. Kanehashi, J.F. Stebbins, J. Non-Cryst. Solids 353 (2007) 4001–4010.
[23] D. Coillot, F.O. Mear, H. Nonnet, L. Montagne, Int. J. Hydrogen Energy 37 (2012) 9351–9358.
[24] M.J. Pascual, M.O. Prado, A. Duran, Phys. Chem. Glasses 46 (2005) 512–520.
[25] D.W. Richerson, Modern Ceramic Engineering, second ed., Marcel Dekker, Inc., New York, USA, 1992.
[26] http://www.qualitydigest.com/jan99/html/body_weibull.html.
[27] W.R. Taylor, Proc. Indian Acad. Sci. 99 (1990) 99–117.
[28] P. Tarte, Spectrochim. Acta A 23 (1967) 2127–2143.
[29] S.K. Sharma Jr., H.S. Yoder, D.W. Matson, Geochchim. Comochim. A 52 (1988) 1961–1967.
[30] K.E. Kelsey, J.R. Allwardt, J.F. Stebbins, J. Non-Cryst. Solids 354 (2008) 4644–4653.
[31] M.J. Pascual, V.V. Kharton, E.V. Tsipis, A.A. Yaremchenko, C. Lara, A. Duran, J.R. Frade, J. Eur. Ceram. Soc. 26 (2006) 3315–3324.
[32] R.A. Young, Introduction to the Rietveld Method, in: R.A. Young (Ed.), The Rietveld Method. International Union of Crystallography Monographs on Crystallography, vol. 5, Oxford University Press, Oxford, 1993, pp. 1–39.
[33] S.R. Choi, N.P. Bansal, A. Garg, Mater. Sci. Eng. A 460–461 (2007) 509–515.
[34] R.G. Kuryaeva, Glass Phys. Chem. 35 (2009) 378–383.
[35] J. Murdoch, J. Stebbins, I. Carmichael, A. Pines, Phys. Chem. Miner. 15 (1988) 370–382.
[36] J.K. Mackenzie, R. Shuttleworth, Proc. Phys. Soc., London, Sect. B 62 (1949) 833.
[37] M.J. Toplis, D.B. Dingvell, Geochim. Cosmochim. Acta 68 (2004) 5169–5188.
[38] K. Matsuai, N. Ohmichi, M. Ohgai, J. Am. Ceram. Soc. 88 (2005) 3346–3352.
[39] L. Zhang, J.A.V. Orman, D.J. Lacks, Am. Mineral. 94 (2009) 1735–1738.
[40] A.A. Omar, S.A.M. Abdel-Hameed, Ceramics - Silikáty 53 (2009) 171–179.
[41] M.K. Mahapatra, K. Lu, Mater. Sci. Eng., R 67 (2010) 65–85.
[42] T. Zhang, Q. Zou, F. Zeng, S. Wang, D. Tang, H. Yang, J. Power Sources 216 (2012) 1–4.